AGU PUBLICATIONS

JGR

Journal of Geophysical Research: Planets

RESEARCH ARTICLE
10.1002/2015JE004895

Key Points:
- Clay minerals in visited dried lakes consist mainly of illite/muscovite and smectite
- Large desiccation fractures probably require water table retreat
- VIS-NIR spectroscopy is not optimal for characterization of lacustrine/playa deposits

Correspondence to:
M. R. El-Maarry,
mohamed.elmaarry@space.unibe.ch

Citation:
El-Maarry, M. R., W. A. Watters, Z. Yoldi, A. Pommerol, D. Fischer, U. Eggenberger, and N. Thomas (2015), Field investigation of dried lakes in western United States as an analogue to desiccation fractures on Mars, *J. Geophys. Res. Planets, 120*, 2241–2257, doi:10.1002/2015JE004895.

Received 9 JUL 2015
Accepted 24 NOV 2015
Accepted article online 27 NOV 2015
Published online 21 DEC 2015

©2015. American Geophysical Union. All Rights Reserved.

Field investigation of dried lakes in western United States as an analogue to desiccation fractures on Mars

M. R. El-Maarry[1], W. A. Watters[2], Z. Yoldi[1], A. Pommerol[1], D. Fischer[3], U. Eggenberger[4], and N. Thomas[1]

[1]Physikalisches Institut, University of Bern, Bern, Switzerland, [2]Whitin Observatory, Department of Astronomy, Wellesley College, Wellesley, Massachusetts, USA, [3]Institute of Geography, University of Bern, Bern, Switzerland, [4]Institute of Geological Sciences, University of Bern, Bern, Switzerland

Abstract Potential Desiccation Polygons (PDPs), tens to hundreds of meters in size, have been observed in numerous regions on Mars, particularly in ancient (>3 Gyr old) terrains of inferred paleolacustrine/playa geologic setting, and in association with hydrous minerals such as smectites. Therefore, a better understanding of the conditions in which large desiccation polygons form could yield unique insight into the ancient climate on Mars. Many dried lakebeds/playas in western United States display large (>50 m wide) desiccation polygons, which we consider to be analogues for PDPs on Mars. Therefore, we have carried out fieldwork in seven of these dried lakes in San Bernardino and the Death Valley National Park regions complemented with laboratory and spectral analysis of collected samples. Our study shows that the investigated lacustrine/playa sediments have (a) a soil matrix containing ~40–75% clays and fine silt (by volume) where the clay minerals are dominated by illite/muscovite followed by smectite, (b) carbonaceous mineralogy with variable amounts of chloride and sulfate salts, and significantly, (c) roughly similar spectral signatures in the visible-near-infrared (VIS-NIR) range. We conclude that the development of large desiccation fractures is consistent with water table retreat. In addition, the comparison of the mineralogical to the spectral observations further suggests that remote sensing VIS-NIR spectroscopy has its limitations for detailed characterization of lacustrine/playa deposits. Finally, our results imply that the widespread distribution of PDPs on Mars indicates global or regional climatic transitions from wet conditions to more arid ones making them important candidate sites for future in situ missions.

1. Introduction

There are currently >1000 detections from orbiting imaging spectrometers of hydrous minerals on the surface of Mars, which are widespread, yet concentrated in the Southern Highlands (see *Carter et al.* [2013] for the global analysis). These detections are dominated by smectites, which are a special family of phyllosilicates with high affinity for water and various formation pathways that mostly require liquid water activity. Many studies of smectite exposures and hydrous minerals, in general, have reported their association with polygonal fracture patterns, which were commonly regarded as a potential result of the desiccation of the once water-saturated smectite-bearing deposits [e.g., *Ehlmann et al.,* 2008, 2009; *Wray et al.,* 2010, 2011; *Erkeling et al.,* 2012; *Bishop et al.*, 2013; *McKeown et al.*, 2013; *El-Maarry et al.,* 2013, 2014].

El-Maarry et al. [2014] showed that potential desiccation polygons (PDPs) are a common feature in phyllosilicate-bearing terrains attaining size scales that range from centimeters to tens of meters wide using images from the High Resolution Imaging Experiment (HiRISE) [*McEwen et al.*, 2007] and currently active rovers (Figure 1). Most PDPs currently observed from orbit range in diameter from 1 to 30 m. However, patterns that are in the submeter range are visible as well in certain locations on Mars that have been investigated in situ by rover missions such as the Mars Exploration Rover "Opportunity" at Meridiani [*Mclennan et al.,* 2005; *Watters et al.,* 2011] and the Mars Science Laboratory "Curiosity" at Gale Crater [*Grotzinger et al.*, 2014]. PDPs are generally flat, lacking raised rims or centers, and are most often observed in light-toned units, with respect to the surrounding terrain. The polygonal patterns usually subdivide as a result of secondary or multiple generations of cracks, which usually require images with submeter spatial resolution to identify.

PDPs are mostly associated with Fe/Mg smectites- or vermiculites-bearing sedimentary deposits. However, they have also been observed in deposits that show spectral signatures of chlorides, Al-rich smectites, and

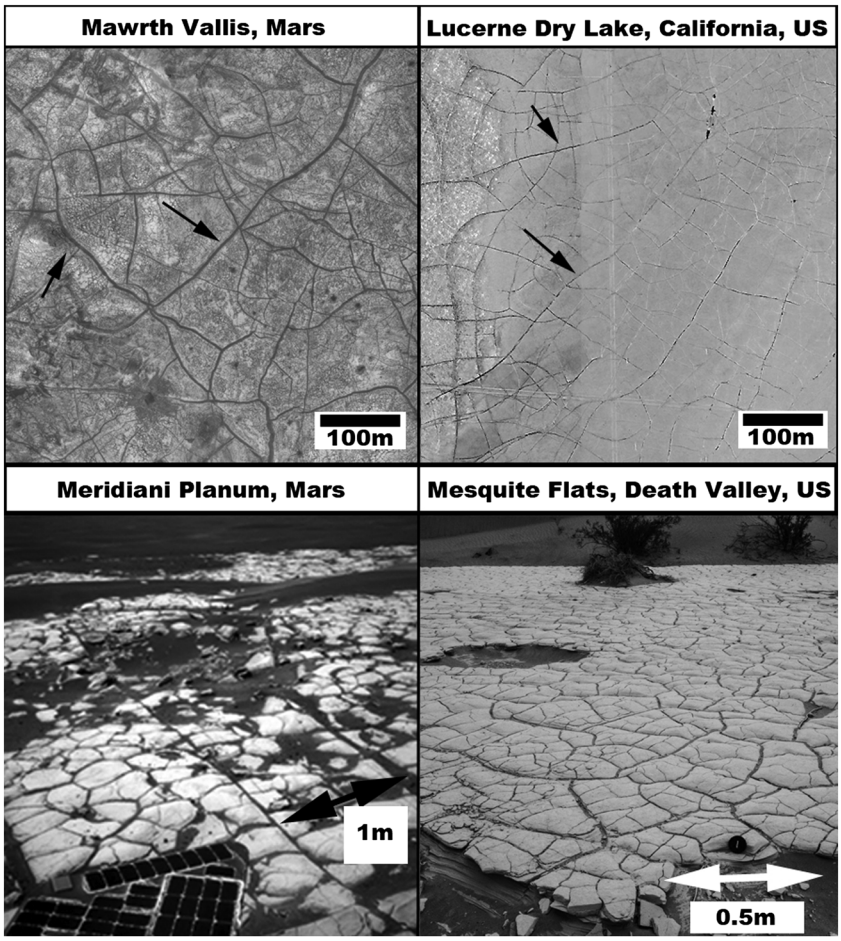

Figure 1. Potential desiccation polygons **(**PDPs) on Mars in comparison to desiccation polygons on Earth. (left column) Mars displays PDPs that span a wide size range from centimeters to hundreds of meters. Arrows in the figures showing large features point to the longest and largest sinuous fractures in the two locations. Image sources for Mawrth Vallis: HiRISE image PSP_006755_2030, Meridiani Planum: Navcam image 1N185802127EFF64EZP1700R0M1, Lucerne Valley: Google Earth, and Mesquite Flats: image acquired by the authors for this study. (right column) Earth images have been intentionally gray scaled for better comparison. For additional information about the Terrestrial images, refer to Table 1 and text.

less commonly of kaolinites and carbonates [*El-Maarry et al.*, 2014]. Notable regions showing PDPs include Mawrth Vallis [e.g., *McKeown et al.*, 2013], Nili Fossae [e.g., *Ehlmann et al.,* 2008, 2010], Libya Montes [e.g., *Erkeling et al.*, 2012; *Bishop et al.*, 2013], Margratifer and Sirenum Terra [e.g., *Osterloo et al.,* 2010*; El-Maarry et al.,* 2014], and chloride-bearing terrains [*El-Maarry et al.*, 2013]. Since the vast majority of phyllosilicate signatures is located in Noachian-aged terrains [*Bibring et al.*, 2006; *Carter et al.*, 2013], which is an era of debatable climatic conditions, investigating the processes that create PDPs in association with these mineral assemblages can constrain the climatic conditions during the time of their formation.

Of particular relevance to this work, numerous recent studies [*Osterloo et al.,* 2008, 2010; *Glotch et al.*, 2010; *Ruesch et al.*, 2012; *El-Maarry et al.*, 2013] suggest that many chloride-bearing terrains, which are also commonly associated with PDPs [*El-Maarry et al.*, 2013], have a lacustrine/playa origin. Incidentally, many playas and dried lakebeds also display large (>50 m wide) desiccation polygons, in particular in western United States in the California/Nevada region [*Neal et al.*, 1968]. Therefore, a study of these regions as an analogue for locations displaying PDPs on Mars is essential to understand better these features. To that end, we report here on the results of fieldwork that was carried out mainly in the summer of 2014 at seven dried lakes/playas in California, U.S., including a number of sites in the Death Valley National Park (DVNP).

Table 1. List of Sites Visited for Fieldwork

#	Location	Coordinates	Main Characteristics
1	Lucerne Lake (San Bernardino)	Site #1: 34°29′45.70″N, 116°57′8.60″W Site #2: 34°30′20.40″N, 116°54′55.20″W	#1: Vegetation-free large desiccation polygons (DPs) and salty, heaved soil #2: Older vegetation-filled large DPs
2	Coyote Lake (San Bernardino)	35°4′11.27″N, 116°43′41.11″W	Old vegetation-filled large DPs less salty and harder than Lucerne
3	Soggy Lake (San Bernardino)	34°27′7.02″N, 116°41′15.40″W	Large vegetation-free DPs in hard sediments
4	North Panamint Lake (DVNP)	36°24′22.95″N, 117°24′53.39″W	Old vegetation-filled large DPs
5	Mesquite flats (DVNP)	36°36′36.57″N, 117°6′45.93″W	Small centimeter-sized DPs in numerous thin outcrops between the Mesquite dunes
6	Racetrack Playa (DVNP)	36°41′39.1″N, 117°34′03.2″W	Small centimeter-sized DPs in hard lakebed
7	Deep Springs Playa (Inyo)	37°16′31.63″N, 118°2′18.24″W	Salt-crusted playa with salt polygons (No DPs)

2. Methods

2.1. Field Methods and Sample Acquisition

The western United States contains many playas and dried lakes. Among these, a small subset of these locations displays large desiccation fractures (see *Neal et al.* [1968] for a comprehensive review). Moreover, a significant number of these sites are generally inaccessible to the public due to their association with U.S. military air bases. Nonetheless, a few sites are freely accessible and relatively easy to reach. For this study, seven sites were chosen (Table 1 and Figures 2–4) that cover a wide range of surface morphologies in order to carry out a geological and compositional comparison. For instance, Coyote and Lucerne dried lakes display

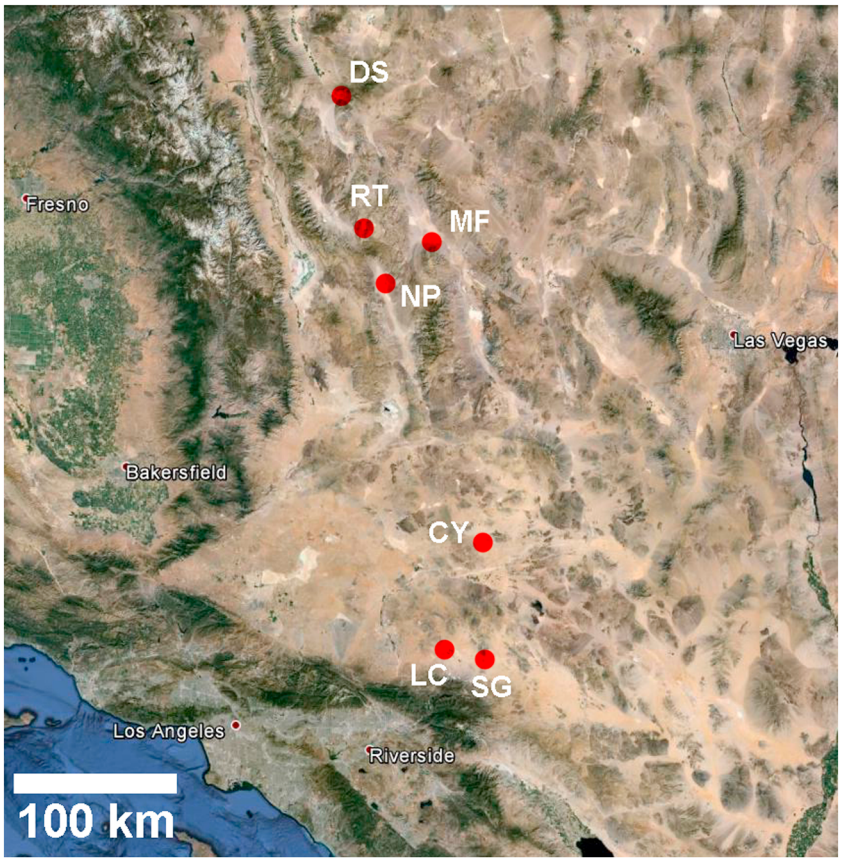

Figure 2. Google Earth view covering parts of California and Nevada showing the locations of dried lakes visited in this study, which include Deep Springs (DS), Racetrack Playa (RT), Mesquite Flats (MF), North Panamint (NP), Coyote (CY), Lucerne (LC), and Soggy (SG) dried lakes/ playas. Image credit: Google Earth.

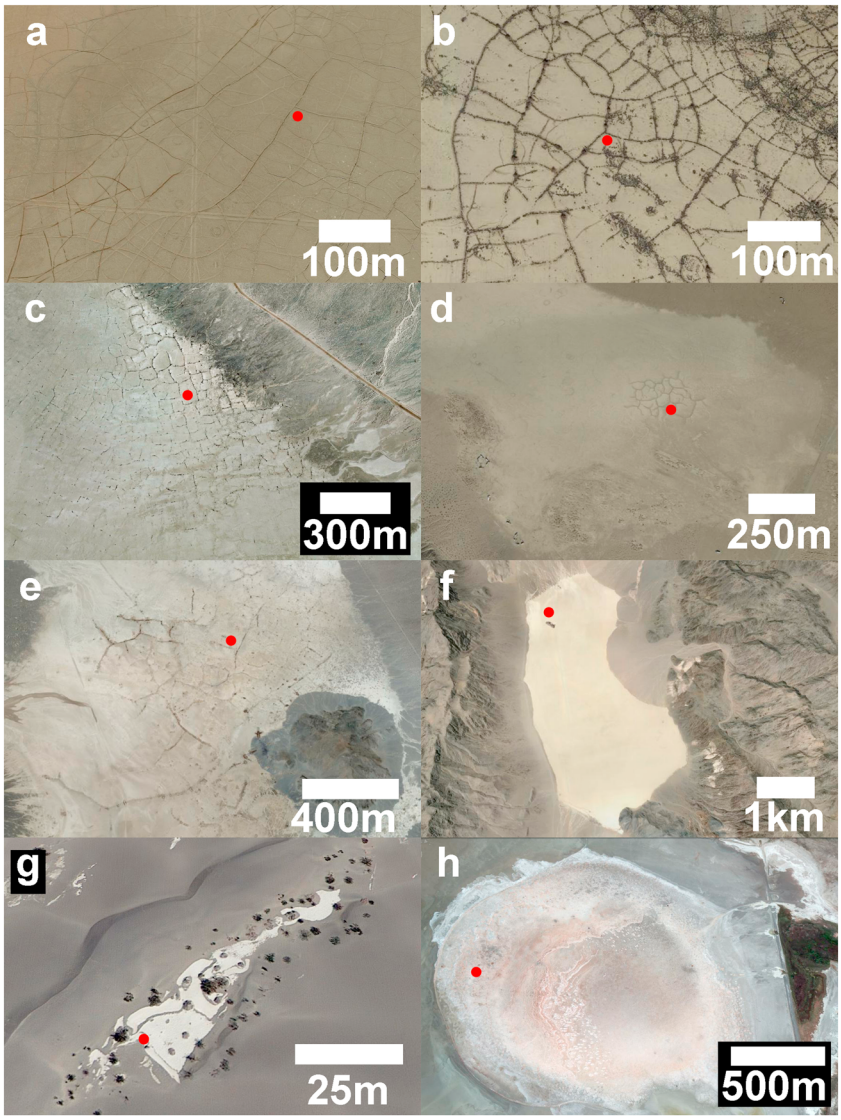

Figure 3. Google Earth view of locations visited in this study, which encompass (a and b) Lucerne (two locations), (c) Coyote, (d) Soggy, (e) North Panamint, (f) Racetrack, (g) Mesquite dunes, and (h) Deep Springs. The red dots show the approximate location of acquired samples. More information is available in Table 1. Credit: Google Earth.

large polygonal fractures (Figure 3) but differ in their vegetation state with Lucerne showing far less vegetation (Figure 4). On the other hand, Mesquite Flats and Racetrack Playa (both in the DVNP) show only small centimeter-sized polygons, whereas the Deep Springs Playa shows no desiccation polygons.

In terms of geography, three of these sites are located in San Bernardino County (Coyote, Lucerne, and Soggy), three are located in DVNP (Mesquite, Racetrack, and North Panamint), and one location in Inyo Country (Deep Springs). In order to study and collect samples from the DVNP sites, we acquired a research permit. However, our initial permit for our visit in July 2014 only included the Racetrack and North Panamint sites due to the National Park's safety concerns with regard to sea level sites, such as Mesquite, in the summer. Therefore, a supplementary permit was acquired specifically for the Mesquite region in winter 2014.

The fieldwork generally consisted of two main tasks: (1) characterizing the surface morphology of the site mainly through imaging using commercial digital cameras (Figure 4), and (2) collecting samples directly from the surface and ~15–30 cm deep (Figure 5) in order to assess possible vertical variation and effect of surface

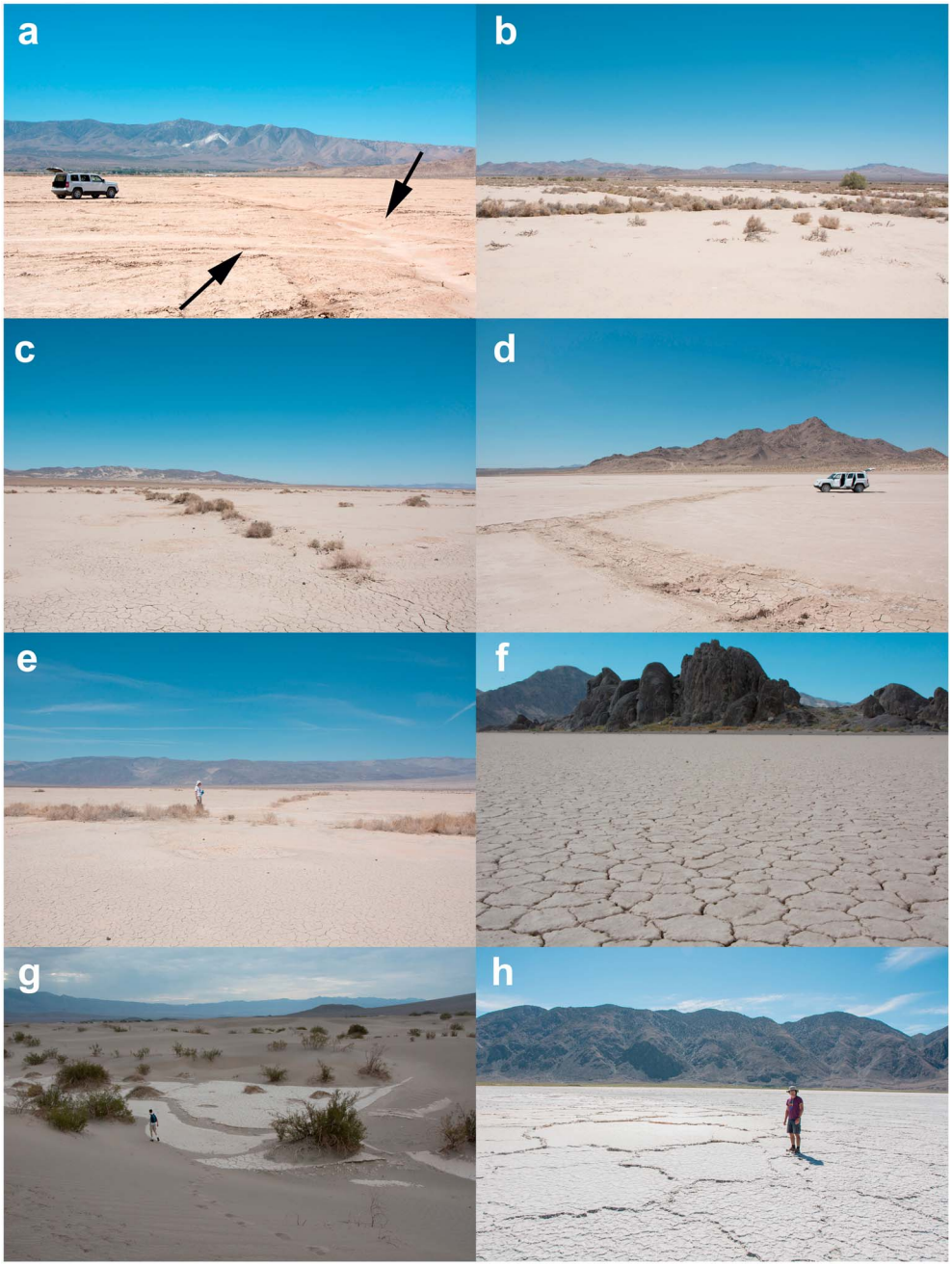

Figure 4. Field images from the visited sites. (a) Lucerne site #1 showing two intersecting fractures (arrows). Note the car for scale (b) Lucerne site #2 east of site #1 showing older cracks that have been filled by vegetation further accentuating the pattern as viewed from air (see Figure 2b). The observed vegetation is approximately knee high. The fracture across the image is ~30 m long. (c) Coyote Lake showing a similar vegetation infill accentuating the cracks. Here too, the observed vegetation is approximately knee high. The fracture along the image is ~100 m long. (d) Soggy Lake showing two intersecting cracks. Note the car for scale. (e) North Panamint showing a similar vegetation infill to Coyote and Lucerne #2. The second author is shown for scale. (f) Racetrack Playa. Polygons in the foreground are ~10 cm wide. In the background the 22 m high "Grandstand" dolomitic outcrop is visible. (g) Mesquite location among the Mesquite dunes in Death Valley. For a close-up refer to Figure 1. (h) Deep Springs Playa showing salt polygons. The first author is shown for scale.

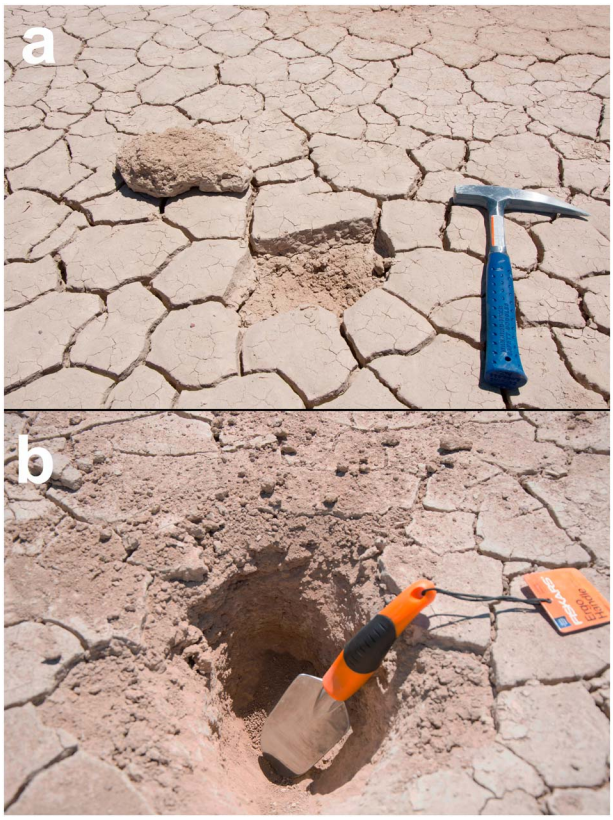

Figure 5. Sampling method for acquiring the field samples. The samples were taken from the (a) surface and at (b) 15–30 cm deep. The deep samples were directly collected from the walls to avoid contamination from surface infill. The images shown here are for samples acquired in Coyote Lake (Table 1, section 3.1.2.), which shows a centimeter-thick fractured and indurated crust overlying compact, nonfractured, fine-grained material.

weathering. The approximate locations where samples were collected are highlighted in Figure 3. The choice of sampling location was generally governed by two factors: (a) proximity to large desiccation fractures as observed from mostly aerial surveys (Figure 3), which did not necessarily correspond to a particular part of the lake basin (such as its center or margins), and (b) proximity to routes accessible by car in order to limit the distance traversed on foot for safety concerns given the high summer temperatures at the time. Two 150–300 g samples were acquired from each site (one surface, one 15–30 cm deep), except for Lucerne Lake, which required sampling from two sites corresponding to the different fracture settings (the old and vegetated versus fresh-looking nonvegetated fractures, Figures 3 and 4). The samples were collected roughly from the polygon centers with small shovels and stored in tightly sealed plastic bags where they remained till the lab analysis phase. For the sites that displayed an indurated upper crust (Figure 5), care was taken to include only the crust in the surface sampling. Afterward, the shovels were used to dig till 15–30 cm deep where the sample was acquired directly from the trench wall to avoid contamination as much as possible from surface debris infill (Figure 5).

2.2. Lab Analysis

The lab analysis consisted of three main techniques: (1) X-ray diffraction (XRD) analysis to derive chemical composition and mineralogy, (2) Laser Diffraction (LD) to derive particle-size distribution, and (3) Visible-Near-Infrared (VIS-NIR) analysis to characterize the spectral properties and to assess similarities and differences with Martian remote sensing measurements [see *El-Maarry et al.*, 2014]. Below, we briefly explain the methods in more detail.

2.2.1. XRD Analysis

As a first step, the samples were milled for 1 min using a tungsten-carbide vibratory disk mill, in order to produce a coarse-grained powder, and then dried overnight in an oven at 50°C. The samples were then split into one portion for the clay mineralogy analysis and another for the basic mineralogy.

To measure the clay mineralogy, 15 g was mixed with NH_4OH 0.01n to prevent coagulation and dispersed for 6–10 min ultrasonically and then poured into Atterberg cylinders. The cylinders were filled by NH_4OH 0.01n to create a sedimentation height of ~20 cm and then left for ~16 h. During that time, 10% diluted Calgon (sodium hexametaphosphate) was added to any of the cylinders that displayed flocculation. Afterward, the suspended clay fraction ($<2\ \mu m$) was separated and acidified with 2n HCl, centrifuged (2500 rpm, 5 min-cycles) and washed with distilled H_2O. Then the clays were saturated with 2n $CaCl_2$ for 30 min. The remaining Ca^{2+} cations were removed by rinsing and centrifuging 3 times with distilled H_2O. The remaining slurry was dispersed again ultrasonically and spread over three glass plates for oriented sedimentation. First plate was air dried, the second one was saturated with ethylene glycol at 50°C overnight to check for swelling clays, and the third specimen was heated to 550°C for 1 h to distinguish kaolinite from chlorite. The three

orientated specimens of each sample were measured on a Philipps PW3710 XRD unit with Cu Kα radiation at 40 kV/40 mA. Reflections from 4° 2Θ to 20° 2Θ at 0.02°/step were recorded with an acquisition time of 1 s/step. The relative amount of montmorillonite, kaolinite, chlorite, and illite was determined by their relative peak height.

To measure the basic mineralogy, 3 g of each dried and milled sample was simply mixed and homogenized with 0.3 g LiF as an internal standard for phase quantification. The samples were disorientated prior to duplicate measurements on a PANalytical™ CubiX^3 X-ray diffractometer (http://www.panalytical.com/CubiX3.htm) with Cu Kα radiation at 45 kV/40 mA using a monochromator. The range from 4° to 60° 2Θ at 0.02°/step was recorded with an acquisition time of 1 s/step. The quantitative abundance (wt %) of the basic minerals was calculated based on the internal standardization (LiF), and semiquantitative abundances of additional phases were derived by Rietveld analyses with PANalytical™ HighScore Plus software package.

2.2.2. LD Analysis

In order to prepare the samples, the soil aggregates in the samples were gently crushed in a mortar and sieved to 2 mm mesh size. Three grams of soil was suspended in 30 mL of distilled water and treated with ultrasound for 5 min. Subsequently, the samples were centrifuged (3000 rpm, 5 min cycles), and the supernatant discarded. This procedure was repeated 3 times to remove all soluble salts. In order to remove organic matter the soil samples were treated with 10 mL of 30% H_2O_2 overnight. Later, the samples were washed twice with distilled water to remove the remaining H_2O_2. Finally, the soil samples were exposed to chemical dispersion by adding 20 mL of sodium hexametaphosphate (33 g L^{-1}) and sodium carbonate (7 g L^{-1}), and shaking overnight.

The particle-size distribution was measured on a Mastersizer 2000 system equipped with the Hydro 2000S dispersion unit (http://www.malvern.com/en/products/product-range/mastersizer-range/default.aspx) using the Laser Diffraction Method where upon illumination of a particle a spatial intensity distribution of the scattered light is generated as function of its size [e.g., *McCave and Syvitski*, 1991]. The settings of the instruments were adapted according to *Ryzak and Bieganoski* [2011]. A minimum of three aliquots of every sample were analyzed, and the average distribution pattern calculated. The grain size distribution was classified using the three main classes of clay (<2 μm), silt (2–63 μm), and sand (63–2000 μm).

2.3. VIS-NIR *Spectral Analysis*

The spectral measurements presented in this study were acquired using the Simulation Chamber for Imaging the Temporal Evolution of Analogue Samples (SCITEAS) [*Pommerol et al.,* 2015]. This small thermal vacuum chamber allows exposing large (>10 cm in diameter and thickness) samples to low temperature and pressure conditions. The surface state of the sample can be continuously monitored by visible and near-infrared hyperspectral imaging through a large window in the center of the upper lid. The hyperspectral system can also be used, as in this study, with the sample under ambient laboratory conditions. During the spectral measurements, the samples were illuminated using a monochromatic light from a 100 W Quartz Tungsten Halogen lamp. The scattered light from the sample was measured using a combination of two cameras: a 1.4 megapixel scientific grade camera (model TSI 1500M-GE from Thorlabs) imaging at the wavelength range of 0.38–1.08 μm and a near-infrared camera model Xeva-2.5-300 from Xenics, which has a high sensitivity over the 0.85–2.5 μm wavelength range. All measurements were calibrated relative to a reference surface made of Spectralon (Labsphere). More details related to the SCITEAS setup are presented in *Pommerol et al.* [2015]. For the purposes of this study, we have tuned the hyperspectral system to increase its spectral resolution in the NIR while optimizing its signal-to-noise ratio at short and long wavelengths (reaching ~400) in order to mimic the characteristics of the spectra recorded by the Compact Reconnaissance Imaging Spectrometer for Mars (CRISM) instrument (see section 1).The spectral resolution varies from 6.5 to 13 nm full width at half maximum from the VIS to the NIR, and the NIR spectra are acquired with a spectral sampling of 6 nm, which is comparable to 6.55 nm for CRISM [*Murchie et al.,* 2007].

3. Results

3.1. Polygons Morphology and Other Features

3.1.1. Lucerne Dry Lake (San Bernardino County)

Lucerne Dry Lake is an irregularly shaped dry lakebed, approximately 3 × 7 km in size, located in the southern Mojave Desert of California ~17 km north of the San Bernardino Mountains [*Rubin et al.*, 2000]. The CA-247 S/

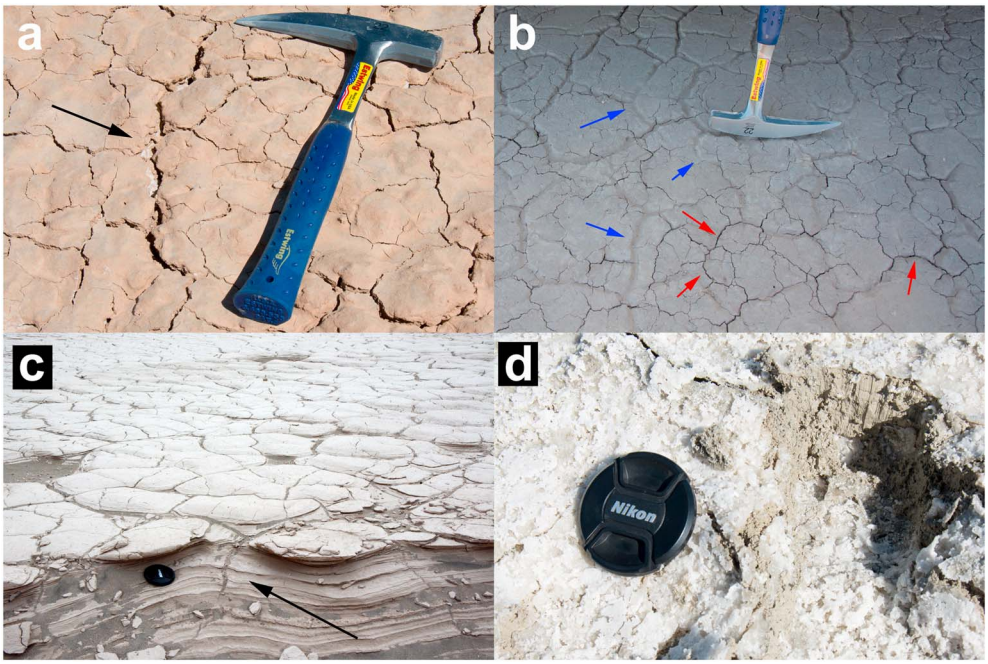

Figure 6. Special features encountered in some of the visited sites: (a) salt concentrations in the cracks observed in Lucerne Lake site #1. (b) Small centimeter-sized polygonal fracture patterns in Coyote Lake showing new (red arrows) and old/healed (blue arrows) cracks interlaced, which is indicative of dry-wet cycles. (c) Fine-laminated mudstone displaying centimeter-sized cracks in Mesquite Flats. (d) View of the dark muddy slurry underlying the bright salt crust in Deep Spring Lake.

Barstow Road cuts through the lakebed and roughly divides it into an eastern and western part. The western part of the lake lacks vegetation, yet displays some of the most remarkable fracture patterns (see Figure 1). On the other hand, the eastern side shows more vegetation, which accentuates older fracture patterns.

Unfortunately, there is little by way of detailed fieldwork in the literature for the majority of the visited sites. However, a number of geophysical and lithological logs for selected sites are available through the public records of the U.S. Geological Survey (USGS). For instance, in *Dockter* [1980a], a stratigraphical cross section is defined through drilling down to ~100 m deep. According to this report, the uppermost 30 m is dominated by calcareous clays with minor (not exceeding 5%) amounts of silt and sand. According to *Rubin et al.* [2000], the lakebed has been significantly affected by deflation processes that involve lifting and removal of unconsolidated clay-size and silt-size particles from the lake surface by wind erosion consistent with the occurrence of clay and silt dunes along its margins.

Viewed from the ground, the two sides of the lake show different surface morphologies. The western side is less consolidated, almost fluffy and heaved in some parts, and shows a progressive subdivision of fractures creating polygons of variable size that range from centimeter- to meter-sized patterns. The larger patterns as viewed from orbit are composed of shallow (almost ankle deep) linear troughs tens of centimeters wide. These shallow troughs probably rest on top of fractures whose depth is unconstrained. The surface and shallow subsurface show patches of evaporite deposits particularly within the fractures (Figure 6a). On the other hand, the eastern side displays a more indurated surface and preferential growth of vegetation within old fractures. In both sites, small centimeter-sized polygonal fractures are visible and show highly irregular fracture intersections. The fractures themselves are mostly nonlinear and, along with the irregularity of fracture intersection, indicate numerous dry-wet cycles [e.g., *Tang et al.*, 2008; *Goehring et al.*, 2010; *Goehring*, 2013].

3.1.2. Coyote Dry Lake (San Bernardino County)

Coyote Dry Lake is a dry lakebed in the Mojave Desert ~24 km northeast of Barstow and ~65 km NE of Lucerne Lake. It is accessible through the Interstate I-15 N and the Alvord Mountain Road but requires a 4×4 car for some parts of the route. The lakebed is approximately 10 by 6 km at its widest point. It is

sparsely vegetated and displays high concentrations of dark volcanic tuffs and pumice at the lake margins, which are probably entrained by episodic surface runoff from the surrounding highlands and eventually settle on the lakebed.

As with Lucerne, similar drilling-based lithological and geophysical assessments show that the uppermost ~70 m of the stratigraphical column is dominated by stratified calcareous clays before giving way to more gravel- and sand-dominated layers [*Dockter*, 1980b]. More recent USGS gravity surveys of the region reveal that the sediments filling the Coyote Lake basin are >1000 m thick [*Jachens and Langenheim*, 2014].

Most of the lakebed is polygonally patterned. However, the well-defined patterns are located in the eastern central part of the lakebed (Figure 3c). Aerial survey images show that the large polygons reach sizes of 50–90 m in width. The fractures themselves are accentuated by the preferential growth of vegetation within the fractures similar to the eastern side of Lake Lucerne (i.e., Lucerne site #2, Figure 4c).

From the ground, small centimeter wide (~8–20 cm) polygons are visible as well as smaller irregular cracks, which could be initial subcracks formed shortly after drying. In contrast to the predominantly T junctions (or orthogonal intersections) of the large fractures viewed from aerial surveys, smaller polygons on the ground form irregular patterns of predominantly Y junctions. Lighter-toned patterns of healed fractures from previous dry-wet cycles interlace the fractured patterns (Figure 6b), which is consistent with the prevalence of Y junctions as crack intersections tend to gradually evolve from T to Y junctions with dry-wet cycles [e.g., *Tang et al.*, 2011].

The small fractures are only a few centimeters deep (with a fracture depth-to-spacing ratio of ~1:5) and divide the lakebed into two main vertical horizons: a centimeter-thick fractured and indurated crust overlying compact, nonfractured, fine-grained material (Figure 5). Finally, unlike the Lucerne location (site #2), many of the vegetated areas are heaved to variable heights even exceeding shoulder height in one location.

3.1.3. Soggy Dry Lake (San Bernardino County)

Soggy Dry Lake is small dry lakebed measuring ~1 km by 2 km at its center. It lies ~25 km SE of the Lucerne site and is readily accessible from the CA-247 S/Old Woman Springs Road. A detailed stratigraphical column down to ~50 m deep is reported in *Dockter* [1980c]. According to this report, the surface down to ~1.5 m is dominated by silt and sand followed mainly by clays for ~25 m before giving way to silts and sandy layers for the rest of the stratigraphical column.

Images from orbit show that only a small portion (roughly 200 m^2) of the lakebed displays large polygonal patterns that are ~40 m wide. From the ground, these polygons are composed of wide troughs similar to the ones encountered in Lucerne site #1. However, the sample acquisition phase revealed a much more indurated surface than what was encountered in Lucerne. In fact, the ground was very hard to dig into in comparison to the other sites visited in this campaign, which suggests that this site is one of the driest lakebeds visited.

Similar to previous sites, the ground is dominated by centimeter-sized polygonal fractures with lighter-toned interlaced patterns suggestive of multiple dry-wet cycles.

3.1.4. North Panamint Lake/Playa (DVNP)

North Panamint Lake or playa is situated in Panamint Valley but is nonetheless within the confines of the DVNP and is separated from Death Valley by the Panamint Range to the East. The lakebed is dominated by clays, fine-grained silt, and minor sands [*Motts and Carpenter*, 1968; *Messina et al.*, 2005]. According to *Neal et al.* [1968], the playa contains lacustrine sediments of the Pleistocene-aged Lake Panamint at depth. North Panamint is typical of numerous southwestern dry lakebeds, in that it contains several common geomorphic features, including solution depressions, drain holes, mud volcanoes, phreatophyte, and spring mounds [*Messina et al.*, 2005].

Messina et al. [2005] made a detailed investigation of the large fractures in the playa and concluded that most of the fissures observed are a result of desiccation (aided by their fortuitous experience of witnessing a fissure in the process of formation after a flash flood in May 1999). However, some fissures appear to be tectonically induced because of their anomalous orientation relative to the other desiccation fractures, which form polygonal patterns, and are radially aligned and parallel or subparallel to the playa boundary.

The fieldwork was conducted in the northern side of the playa since images from aerial surveys suggested that this location displayed the most developed fracture systems. The location is accessible through CA-190 W

(which cuts through the basin and divides it into a northern and southern part) and a dirt road that requires a 4 × 4 car in some sections.

From the ground, the polygonal patterns resemble those observed in Coyote and Lucerne site #2 in displaying substantial vegetation growth within the fractures. However, in our location, the vegetation appeared to grow in considerably wider (~2–3 m wide) bands than what was observed elsewhere. In addition, similar small-sized polygons composed of nonlinear fractures creating Y junction intersections are ubiquitous.

3.1.5. Racetrack Playa (DVNP)

Racetrack Playa is a flat ~ 4.5 km by 2 km lakebed at its widest part. It is perhaps most famous for its "sliding rocks," which are boulders and cobbles that apparently move across the surface of the playa leaving clear trails [e.g., *Sharp and Carey*, 1976; *Reid et al.*, 1995; *Messina and Stoffer*, 2000; *Lorenz and Jackson* [2014]; *Norris et al.* [2014]]. The playa has even been suggested as an analogue for hydrocarbon lakes on Titan [*Lorenz et al.*, 2010].

As the playa is extremely flat (differing in altitude by 5–10 cm from one end to the other) [*Lorenz et al.*, 2010], it can easily get entirely flooded. When it dries up, small centimeter-sized polygons fill the playa surface and most of the investigators who have carried out fieldwork in the site have noted their constant presence when the lakebed is dry. The polygons are highly regular in size displaying widths in the range of 6–13 cm. However, the fractures themselves are mostly nonlinear, which is suggestive of multiple dry-wet cycles, and form Y junctions similar to other small polygons encountered in other sites. Similar to Coyote, the surface fractures extend vertically down to a few centimeters dividing the lakebed vertically into two layers.

3.1.6. Mesquite Flats (DVNP)

The Mesquite flats occupy one of the lowest elevated areas (~15 m below sea level) in the basin and are easily accessible from the CA-190 road with their own dedicated parking spot ~3 km east of Stovepipe Wells. The area is known better for the sand dunes that currently cover most of the flats. Many locations particularly in the interdune areas (Figure 3g) display light-toned flat terrains that show remarkable polygonal fractures reminiscent of the patterns observed in Meridiani Planum on Mars by the Opportunity Rover (see Figure 1).

Close inspection of a number of these sites shows that the polygonal fractures occur in very fine and laminated mudstone. The fractures form a cracking hierarchy with wider fractures creating larger polygons and vice-versa. The polygons are slightly high centered forming in thin sheets on the surface of the laminated mudstone as observed in numerous available cross sections (Figure 6c) and show a variety of sizes ranging from centimeters to tens of centimeters. Since this location is the subject of a detailed dedicated study, more details about this site will be available in an upcoming manuscript.

3.1.7. Deep Springs Playa (Inyo County)

Deep Springs Lake is a small intermittent pan-shaped playa within a completely closed basin in Inyo County, CA (see *Jones* [1965] for a detailed review of the playa's geology and hydrology). The playa is accessible from the CA-168 road. However, a 4 × 4 car with high clearance and oral permission are required in order to traverse the ~5 km long (and fenced) dirt roads leading from the highway to the playa as they appear to be privately owned by nearby ranches.

The surface of the playa is marked by a thick, porous, variable-colored salt crust broken into irregular polygonal units ranging from a few to tens of meters across (Figure 4h). Earlier researchers have noted similar observations as well [*Jones*, 1965]. Below this thin salt crust, the lakebed is dark, muddy, soft and deformable (Figure 6d), which made it very difficult to stand still in any given area of the surface without sinking. Some regions of the playa surface display small patches of yellowish to reddish colored brines suggesting ongoing, yet slow, evaporation as a result of the high altitude of the playa (~1500 m above sea level) and low annual ambient temperatures [*Jones*, 1965].

3.2. Mineralogy of Acquired Samples

3.2.1. XRD and LD

A summary of the XRD results for samples collected from all sites is presented in Table 2. As mentioned in section 2.1, samples were acquired in each site from the surface and at a depth ranging from 15 to 30 cm deep. This approach helps in assessing the effect of surface weathering and investigating possible subsurface variations.

Table 2. Summary of XRD and LD Analysis on Samples Collected for This Study[a]

	Lucerne Site 1		Lucerne Site 2		Coyote		Soggy		North Panamint		Racetrack		Mesquite	Deep Springs	
	S	D	S	D	S	D	S	D	S	D	S	D	S	S	D+
							XRD								
Calcite	8	8	10	10	5	7	9	9	7	11	11	11	8	1	1
Dolomite	1	1	2	2	0	0	2	3	6	15	7	4	15	5	17
Total carbonates	9	9	12	12	5	7	11	12	13	26	18	15	23	6	18
K-feldspar	6	15	24	12	5	5	5	7	7	12	10	8	10	2	4
Plagioclase	4	5	16	9	4	4	3	5	4	7	6	4	3	9	4
Quartz	4	4	12	9	5	5	8	6	7	6	14	11	7	2	7
Halite		2		x	0.5			x	6	1.5				9	4
Gypsum		xxx								x					
Hornblende			xx	x	x		x	x	x	x	x	x	x		
Pyrophillite									x		xx	x	x		
Analcime					5	6									
Thenardite														36	x
Clay + amorphous content	77	65	36	58	75.5	71	73	70	63	47.5	52	62	57	36	63
Illite/muscovite[b]	71	72	54	51	58	58	66	70	46	38	68	69	52		81
Smectite[b]	10	9	30	33	26	24	14	13	31	39	7	6	37		7
Kaolinite[b]	14	9	6	7	7	0	5	5	7	7	10	25	6		3
Chlorite[b]	5	9	11	10	9	18	16	13	17	16	15	0	5		9
							LD (in % vol)								
Clay (0.02–2 um)	40.8		11.7	13.7	27	33.7	26.7	28.4	17.1	22	18	16.1	15.6		19.5
Fine silt (2–6.3 um)	33.7		26.3	28	24	24.3	27.2	29.7	27.8	26.7	29.5	24	28.4		38.5
Total silt (2–63 um)	52.4		71.7	70.5	52.7	57.6	52.7	59.1	72.5	52.9	68	54.8	78		57.6
Clay + fine silt	74.5		38	41.7	51	58	53.9	58.1	44.9	48.7	47.5	40.1	44		58

[a]XRD Values are given as estimated wt %, while LD estimates are vol%. "S" and "D" correspond to samples acquired at the surface and at a depth of 20–30 cm deep, respectively, except for the Deep Springs sample (D+), which was acquired at ~15 cm deep. Abundances given in "x" symbols are relative estimates since precise abundances could not be measured from the XRD spectra. No LD data were acquired for the surface sample of Deep Springs (or clay analysis), because the sample was salt dominated, nor for the Lucerne Site 1 at depth, because the sample was damaged during preparation.
[b]Abundance normalized to the abundance of the four clay minerals.

From the data presented in Table 2, several trends are observed. With regards to general mineralogy, samples are generally calcareous showing calcite abundances of 6–11 wt % in addition to variable amounts of dolomite ranging from 0 to 15 wt %. The samples collected in DVNP are generally the most abundant in carbonates reaching 26% in the North Panamint dried lake. In addition to carbonates, all sites display moderate to high amounts of K-feldspar and low to moderate abundances of plagioclase. We also observe low to moderate amounts of salts in the samples, which are dominated by chlorides (mainly halite). However, certain localities display significant amounts of gypsum such as the Lucerne site #1 (albeit of undetermined quantity), and thenardite (Na_2SO_4), which is a dominant mineralogical species, along with halite, in Deep Springs Playa. The presence of thenardite in Deep Springs, while unique to our samples, is not surprising since it has been reported before in the region, particularly in Saline Valley ~65 km south of Deep Springs [e.g., *Hardie*, 1968; *Crowley*, 1993].

With regards to clay mineralogy, the dominant clay mineral species appears to be illite/muscovite in nearly all samples (38–81% of the clay content, with a mean of ~61% and a standard deviation of ~11.5%) in addition to significant amounts of smectites and variable amounts of kaolinites and chlorites.

The abundance of clay minerals is not adequately constrained using the XRD technique as the presence of other amorphous species such as organics adds notable uncertainty to the obtained values. Therefore, we utilized LD techniques in order to the get a better estimate of the clay content. The results are similarly summarized in Table 2. Almost all samples are dominated by silt-size grains followed by clays. However, a significant portion of these silts are in the fine silt grain size (2–6.3 um) such that all samples contain a combined amount of clays and fine silt in the volumetric range of ~40–75% with a mean of ~50% and a standard deviation of ~9.5%.

Finally, with regards to vertical variations, all sites show homogeneity in terms of general mineralogy from the surface to deep samples with the exception of North Panamint, which shows a decrease in carbonate

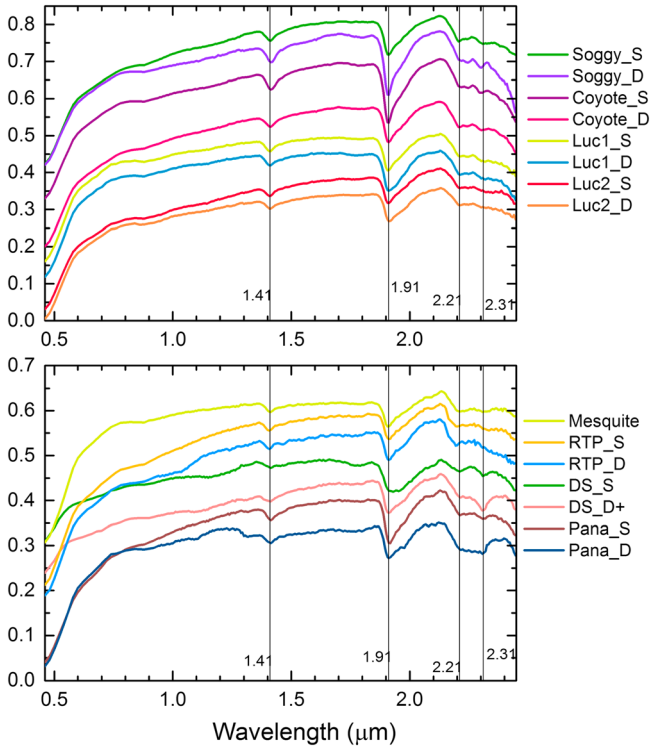

Figure 7. VIS-NIR spectra of field samples as measured in the SCITEAS chamber. (top) The spectra in the San Bernardino County. (bottom) The rest of the samples in the Death Valley National Park and Inyo County. The acronyms/abbreviations are as follows: LUC1: Lucerne Lake site #1, LUC2: Lucerne Lake site #2, RTP: Racetrack Playa, DS: Deep Spring Lake, Pana: North Panamint Lake. Finally, S and D represent "surface" and "deep" samples, respectively. Note the similarities in absorptions in almost all samples.

concentration at the surface, and Deep Springs, in which the salt crusts are significantly different from the subsurface mud. In terms of grain size, there is a clear trend in all the sites where the clay content is lower at the surface, which is consistent with a preferential weathering effect where smaller-sized particles are being eroded or transported more readily, consistent with *Rubin et al.* [2000]'s observation at Lucerne. In fact, the lower abundances of carbonates at the surface of North Panamint with respect to the deep samples could be explained if most of the carbonates in the playa are clay sized, and consequently have been transported away.

3.2.2. VIS-NIR Spectra

The spectra as measured in the SCITEAS chamber are presented in Figure 7 along with a comparison to reference spectra (Figure 8). The references were measured with the same instrument. However, for the mineral references that are identified in the XRD analysis and missing from our inventory (e.g., thenardite), we have utilized spectra from the USGS Digital Spectral Library [*Clark et al.*, 2007].

Most of the samples show similar absorption features where all the samples show deep absorptions at ~1.90–1.91 μm, except for the thenardite-dominated sample (Deep Springs surface sample, DS_S) that shows a broader absorption centered at ~1.93 μm, and most show absorptions of variable depth at ~1.41 μm. The samples may be slightly distinguished from each other by the presence/absence of absorptions near 2.21 and 2.31 μm.

In general, the samples acquired in the San Bernardino and Mojave regions appear to have stronger absorptions than those of the Death Valley region. This difference does not appear to be related to grain size (Table 2), as no discernable trend could be identified in the LD analysis, but instead could indicate that the samples in the Death Valley region are simply less hydrated.

The absorption bands at ~1.41 and 1.91 μm are usually attributed to adsorbed water and hydrated minerals in general [e.g., *Hunt*, 1977]. The 2.21 and 2.29–2.31 μm absorption features generally correspond to Al-OH and Mg-OH or Fe(II)-OH bonds, respectively [e.g., *Clark et al.*, 1990; *Frost et al.*, 2002; *Bishop et al.*, 2002]. Almost all samples show a shoulder at ~2.4 μm, which unfortunately is ambiguous because it is near our detection limit and exhibits higher noise levels. The combination of these five absorptions (i.e., 1.4, 1.9, 2.2, 2.3, and 2.4–2.5) should roughly correspond to illite/muscovite, which dominates the field samples (Table 2) in addition to smectites. Indeed, illite/muscovite and K-mica, in general, display absorption features at 2.2, 2.34–2.35, and 2.45 μm [e.g., *Clark et al.*, 1990], whereas the 2.29–2.32 absorptions are indicative of Fe/Mg smectite [e.g., *Clark et al.*, 1990; *Grauby et al.,* 1994; *Bishop et al.*, 2002]. However, it is important to note that the 2.34–2.35 absorption feature is markedly lacking or highly ambiguous in our spectra despite the dominance of illite/muscovite in our samples. We cannot attribute this ambiguity to instrumental limits because we are able to discern such absorption features in the reference minerals we measured, including illite (IMt_1 in Figure 8), which incidentally matches well with the spectra of the same mineral in the

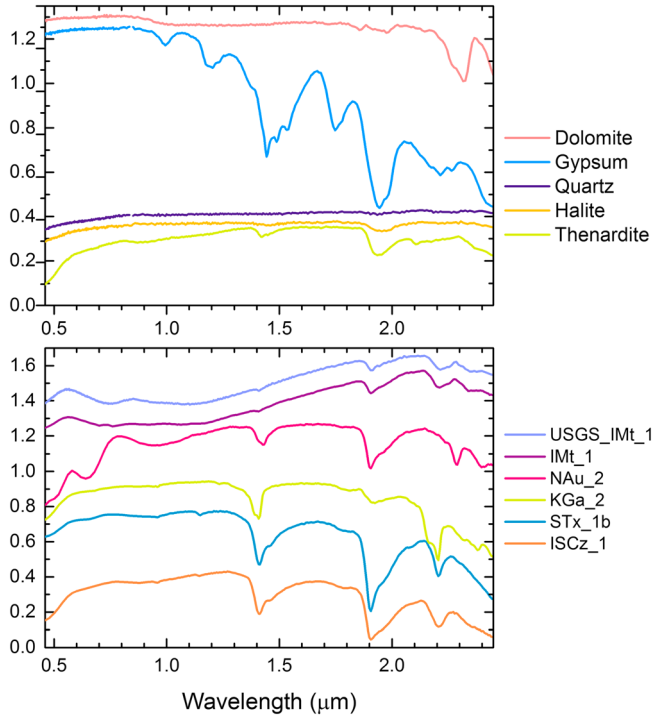

Figure 8. Reference spectra used in this study. (top)The spectra for reference minerals acquired from the Clay Minerals Society measured directly in the SCITEAS chamber. (bottom) The spectra that have been derived from the USGS spectral library [*Clark et al.*, 2007]. The acronyms of the standard clays are the ones used by the Clay Minerals Society and are as follows: NAu_2: Nontronite (Fe-rich smectite), IMt_1: Illite, KGa_2: Kaolinite, STx_1b: Ca-Montmorillonite, and ISCz_1: Illite-smectite mixed layer. Note that the IMt_1 USGS spectra are shown in both figures mainly for comparison with the IMt_1 spectra acquired from SCITEAS.

USGS spectral library (Figure 8). In the absence of such absorptions, we would not be able to identify illite/muscovite in our samples without a priori knowledge.

Other minerals detected in the XRD analysis that should show similar absorptions in at least one of these five absorption bands include carbonates (1.9 and 2.3–2.35) [*Hunt and Salisbury*, 1970; *Gaffey*, 1984], kaolinite (1.4 and a doublet at ~2.2 μm)[*Clark et al.*, 1990; *Petit et al.*, 1999], halite and thenardite (~1.4 and ~1.9 μm) [*Crowley*, 1991], and gypsum (~1.45–1.5, ~1.9, ~2.2, and ~2.4 μm)[*Crowley*, 1991].

4. Discussion

4.1. Conditions for Development of Large Desiccation Fractures

In total, seven different locations were investigated in this study (Table 1). Four of those display large desiccation fractures, two display small centimeter-sized polygons, and one salt-rich playa displays meter-sized salt polygons but no conventional desiccation features. In terms of mineralogy, no discernable trends exist that would distinguish the sites showing large desiccation fractures from the ones that do not. In fact, all locations show roughly a few common attributes: (1) a soil matrix with significant clay and fine silt content (~50% on average), (2) illite/muscovite-dominated clay content (~60% on average of the clay content) with significant amounts of smectite, and (3) carbonaceous mineralogy with variable amounts of salts, mainly as chlorides and in some cases sulfates. This suggests that other, or additional, factors control the development of large desiccation fractures.

Early studies [e.g., *Neal et al.*, 1968] have argued that large desiccation polygons should develop in association with intense evaporation and lowering of groundwater levels rather than simple evaporation from the surface. Testing this idea, *El-Maarry et al.* [2012] demonstrated that large desiccation fractures may indeed form through such a mechanism by modeling the tensile stresses that would develop through lowering of a water table under conditions of hydraulic diffusivity that are commonly associated with clay-dominated deposits and showed that fractures may form in a timescale of 1 to 2 years, which was also in agreement with *Neal et al.*'s [1968] predictions. Therefore, lowering of the water table appears to be a key factor in the formation of large (hundreds of meters in scale) desiccation fractures.

Neal et al. [1968] and *Goetz* [1980] had attributed the lowering of water table levels in regions such as the San Bernardino County to intense irrigation and human consumption, which offers an explanation for the development of large fractures in the sites visited in this particular region. Indeed, regional water table maps for the San Bernardino region [e.g., *Teague et al.*, 2014] (a detailed list of regional water table maps is available through The Mojave Water Agency (http://www.mojavewater.org/regional-water-table.html)) clearly show a decline in water table levels since the 1950s in many regions including the Lucerne dried Lake. It should be noted that similar comprehensive data are unavailable for the two other dried lakes of interest in the County (i.e., Soggy and Coyote), probably due to their relatively more secluded nature.

If indeed water table retreat was a key factor in the formation of large desiccation features, we would assume that such a mechanism has been lacking, at least on the same scale, in the DVNP area, where the Racetrack and Mesquite sites are located. Indeed, geological reports indicate that groundwater underlies most of the Death Valley region and "is probably in a steady state" [*Miller*, 1977] being annually replenished by a 4000 miles^2 drainage area and stream channels during floods despite the extremely dry conditions of the valley (*Miller* [1977], see also *Bedinger and Harrill* [2012] for a more recent report).

In particular, the Mesquite flats are situated in one of the low elevation points of the valley (~15 m below sea level), which makes it a preferred location for groundwater discharge [*Bedinger and Harrill*, 2012]. On the other hand, the high elevation of Racetrack Playa (~1130 m above sea level) places it well above ground water levels but facilitates regular precipitation through heavy downpour or more commonly through snow accumulation in winter [*Lorenz et al.*, 2011]. As a result, these two sites (showing only small centimeter-sized desiccation features) are dominated by surface evaporation processes rather than water table retreat.

With regards to Deep Springs Lake, the only visible polygons on the surface are meter-sized salt polygons. *El-Maarry et al.* [2015] have recently reported using lab experiments that soils mixed with very high concentrations of salt could create an almost impermeable salt crust that acts to slow desiccation rates considerably and may even stop the process entirely [*El-Maarry et al.*, 2015]. Indeed, our experience in the field shows that the subsurface mud beneath the salt crust is retaining its near slurry state. Therefore, we conclude that the high salt contents in the Deep Springs Lake are responsible for the absence of large desiccation fractures.

Finally, although the North Panamint Lake, which shows large desiccation fractures, is currently part of the DVNP, it in fact lies geographically west of Death Valley being separated from it by the North Panamint Mountain Range. Therefore, it is likely that the region was similarly affected by groundwater retreat in agreement with *Messina et al.*'s [2005] conclusions following their investigation of the area. Interestingly, the lowering of the water table in the area may have been anthropogenic similar to other visited sites (e.g., Lucerne), but may also be geologic. During the late Pleistocene, hundreds of meter deep lake is reported to have filled the Panamint Valley during periods of maximum pluvial activity [e.g., *Jayko*, 2005; *Bedinger and Harrill*, 2012]. Therefore, long-term climatic changes leading to lowering of regional water tables may have been partly responsible for the evolution of the dried lake into its current form [*Neal and Motts*, 1967]. This natural long-term climatic variation may have interesting implications for the formation of PDPs on Mars, which we discuss briefly in the next section.

4.2. Identification of Paleolacustrine/Playa Sites on Mars and Implications for Paleohydrology

El-Maarry et al. [2014] showed that PDPs are a common feature in phyllosilicate- and chloride-bearing terrains on Mars. In their study, the spectral evidence for the presence of smectites in combination with PDPs was proposed as a useful tool for identifying paleolacustrine/playa sites, which are of high geological and exobiological significance for future Mars exploration missions, especially future rovers such as the European ExoMars Rover (planned for 2018) and the US-led Mars 2020 mission. Our chemical characterization of field samples acquired from dried lakes/playas displaying large desiccation fractures lends support to the connection between large desiccation polygons and paleolacustrine sites considering the detection of significant amounts of smectites in all field samples. However, these samples appear to be dominated by illite/muscovite, whereas smectites appear to be the more commonly identified hydrous mineral species on Mars. Nevertheless, our spectral analysis using an imaging spectrometer as an analogue to CRISM with roughly similar sampling rate and signal-to-noise ratio shows that it is difficult to identify illite/muscovite in paleolacustrine deposits that similarly contain significant amounts of smectites in addition to other hydrous minerals and salts. Therefore, it is possible that many illite/muscovite-dominated deposits on Mars have gone undetected.

In fact, despite the chemical variability of our samples and their inferred variable hydrological history, most of our samples are very difficult to spectrally distinguish from one another being mostly dominated by the absorption features at ~1.4,1.9, 2.2, and 2.3 μm. In that respect, we consider the current remote sensing VIS-NIR instruments adequate for identifying paleolacustrine/playa deposits. However, a detailed characterization looks nearly impossible in the absence of other tools and experiments that would need to be carried out in situ. It should be noted that *Lynch et al.* [2015] arrived to the same conclusions following their

fieldwork in the Great Salt Lake Desert. Therefore, our conclusions, in this regard, are not new but are in support of theirs.

Furthermore, our work may have important implications for our understanding of the paleohydrology of Mars. Our analysis shows that it is very challenging to distinguish sites that are dominated by surface evaporation from those characterized by groundwater fluctuations through even a detailed mineralogical investigation. In that respect, the presence of large desiccation fractures is a useful tool in inferring the different hydrological histories. By extension, the presence of many sites showing PDPs may suggest a global or multiple local transition phases in the hydrological cycle on Mars where a shift occurred from a period of high liquid water activity (even if transient), possibly pluvial dominated, to periods characterized by slow groundwater table retreat and associated dry conditions at the surface. Thorough dating of the many sites showing PDPs on Mars may reveal whether the transition was global or characterized by multiple fluctuations at a more local or regional scale.

Finally, we regard the sites that have been visited in this study as useful terrestrial analogues that should be investigated further and may act as testing beds for future rovers especially those equipped with drilling capabilities given the high probability that such rovers will be eventually sent to similar locations on Mars because of their high geological and exobiological significance.

5. Summary

We have carried out fieldwork in seven dried lakes and playas in western United States complemented with laboratory analysis of acquired samples in order to understand the conditions in which large (tens to hundreds of meters in size) desiccation fractures and polygons develop on Earth as an analogue for PDPs on Mars. The acquired samples display these common trends: (1) A soil matrix containing a significant amount of clays and fine silt (an average of ~50% by volume), (2) illite/muscovite-dominated clay content (~60% on average) with significant amounts of smectite, (3) carbonaceous mineralogy with variable amounts of salts, mainly as chlorides and in some cases sulfates, and (4) roughly similar spectral signatures in the VIS-NIR range with absorption features at ~1.4, 1.9, 2.2, and 2.3 μm.

Our analysis of the mineralogy and review of the hydrological evolution of the numerous locations suggests water table retreat maybe a key factor in the formation of large desiccation polygons, consistent with previous studies [e.g., *Neal et al.*, 1968; *Goetz,* 1980; *El-Maarry et al.*, 2012]. In addition, the comparison of the mineralogical data to the spectral one further suggests that VIS-NIR remote sensing is adequate in identifying paleolacustrine deposits, yet its usefulness becomes limited if detailed characterization of the lacustrine deposits is needed. Finally, our results imply that the numerous locations on Mars that contain PDPs may indicate global or regional climatic transitions from liquid water-rich conditions to more arid ones.

Acknowledgments

This study was supported by funds from the Swiss National Science Foundation (SNSF) and kind support from the Bern University Research Foundation. The study and sample acquisition in the locations situated in Death Valley National Park were conducted under National Park permits DEVA-2014-SCI-030 and DEVA-2015-SCI-010. We would like to thank Christine Lemp and Despoina Diamontopoulou for their assistance in the lab with the XRD analysis. We also thank Ralph Lorenz and two additional reviewers for their constructive and critical comments and suggestions. All the field photos and data sets presented in this study are available upon request from the lead author. HiRISE images are available in https://hirise.lpl.arizona.edu/, whereas images from Earth orbit and aerial surveys are available freely through Google Earth (https://www.google.com/earth).

References

Bedinger, M. S., and J. R. Harrill (2012), Groundwater geology and hydrology of Death Valley National Park, California and Nevada, Natural Resource Technical Report NPS/NRSS/WRD/NRTR—2012/652.

Bibring, J.-P., et al. (2006), Global mineralogical and aqueous Mars history derived from OMEGA/Mars Express data, *Science*, *312*, 400–404, doi:10.1126/science.1122659.

Bishop, J., J. Madejova, P. Komadel, and H. Froschl (2002), The influence of structural Fe, Al, and Mg on the infrared OH bands in spectra of dioctahedral smectites, *Clay Miner.*, *37*, 607–616, doi:10.1180/0009855023740063.

Bishop, J. L., et al. (2013), Mineralogy and morphology of geologic units at Libya Montes, Mars: Ancient aqueously derived outcrops, mafic flows, fluvial features, and impacts, *J. Geophys. Res. Planets*, *118*, 487–513, doi:10.1029/2012JE004151.

Carter, J., F. Poulet, J.-P. Bibring, N. Mangold, and S. Murchie (2013), Hydrous minerals on Mars as seen by the CRISM and OMEGA imaging spectrometers: Updated global view, *J. Geophys. Res. Planets*, *118*, 831–858, doi:10.1029/2012JE004145.

Clark, R. N., T. V. V. King, M. Klejwa, G. A. Swayze, and N. Vergo (1990), High spectral resolution reflectance spectroscopy of minerals, *J. Geophys. Res.*, *95*(B8), 12,653–12,680, doi:10.1029/JB095iB08p12653.

Clark, R. N., G. A. Swayze, R. Wise, E. Livo, T. Hoefen, R. Kokaly, and S. J. Sutley (2007), *USGS Digital Spectral Library Splib06a*, *Digital Data Ser.*, vol. 231, U.S. Geol. Surv. [Available at http://speclab.cr.usgs.gov/spectral.lib06.]

Crowley, J. K. (1991), Visible and near-infrared (0.4–2.5 μm) reflectance spectra of playa evaporite minerals, *J. Geophys. Res.*, *96*(B10), 16,231–16,240, doi:10.1029/91JB01714.

Crowley, J. K. (1993), Mapping playa evaporite minerals with AVIRIS data: A first report from Death Valley, California, *Remote Sens. Environ.*, *44*(2–3), 337–356, doi:10.1016/0034-4257(93)90025-S.

Dockter, R. D. (1980a), Geophysical, lithologic, and water quality data from Lucerne Dry Lake, San Bernardino County, California, *U.S. Geol. Surv. Open File Rep., 80–1032*.

Dockter, R. D. (1980b), Geophysical, lithologic, and water quality data from Test Well CO-1, Coyote Dry Lake, San Bernardino County, California, *U.S. Geol. Surv. Open File Rep., 80–1031*.

Dockter, R. D. (1980c), Geophysical, lithologic, and water quality data from Soggy Dry Lake, San Bernardino County, California, *U.S. Geol. Surv. Open File Rep., 80–1030*.
Ehlmann, B. L., et al. (2008), Orbital identification of carbonate-bearing rocks on Mars, *Science*, *322*, 1828–1832.
Ehlmann, B. L., et al. (2009), Identification of hydrated silicate minerals on Mars using MRO-CRISM: Geologic context near Nili Fossae and implications for aqueous alteration, *J. Geophys. Res.*, *114*, E00D08, doi:10.1029/2009JE003339.
Ehlmann, B. L., J. F. Mustard, and S. L. Murchie (2010), Geologic setting of serpentine deposits on Mars, *Geophys. Res. Lett.*, *37*, L06201, doi:10.1029/2010GL042596.
El-Maarry, M. R., J. Kodikara, W. Markiewicz, W. Wijessoriya, and N. Thomas (2012), Desiccation mechanism for formation of crater floor polygons on Mars and giant polygons on Earth: Results from a pre-fracture model, *Earth Planet. Sci. Lett.*, *323*, 19–26.
El-Maarry, M. R., A. Pommerol, and N. Thomas (2013), Analysis of polygonal cracking patterns in chloride-bearing terrains on Mars: Indicators of ancient playa settings, *J. Geophys. Res. Planets*, *118*, 2263–2278, doi:10.1002/2013JE004463.
El-Maarry, M. R., W. Watters, N. McKeown, J. Carter, E. Noe Dobrea, J. Bishop, A. Pommerol, and N. Thomas (2014), Potential desiccation cracks on Mars: A synthesis from modeling, analogue-field studies, and global observations, *Icarus*, *241*, 248–268.
El-Maarry, M. R., A. Pommerol, and N. Thomas (2015), Desiccation of phyllosilicate-bearing samples as analogue for desiccation cracks on mars: Experimental setup and initial results, *Planet. Space Sci.*, *111*, 134–143.
Erkeling, G., et al. (2012), Valleys, paleolakes and possible shorelines at the Libya Montes/Isidis boundary: Implications for the hydrologic evolution of Mars, *Icarus*, *219*, 393–413.
Frost, R. L., J. T. Kloprogge, and Z. Ding (2002), Near-infrared spectroscopic study of nontronites and ferruginous smectite, *Spectrochim. Acta, Part A*, *58*, 1657–1668.
Gaffey, S. J. (1984), Spectral reflectance of carbonate minerals and rocks in the visible and infrared (0.35 to 2.55 /am) and its applications in carbonate petrology, PhD thesis, 235 pp., Univ. of Hawaii, Honolulu.
Glotch, T. D., J. L. Bandfield, L. L. Tornabene, H. B. Jensen, and F. P. Seelos (2010), Distribution and formation of chlorides and phyllosilicates in Terra Sirenum, Mars, *Geophys. Res. Lett.*, *37*, L16202, doi:10.1029/2010GL044557.
Goehring, L. (2013), Evolving fracture patterns: Columnar joints, mud cracks, and polygonal terrain, *Philos. Trans. R. Soc. A*, *371*, 20120353, doi:10.1098/rsta.2012.0353.
Goehring, L., R. Conroy, A. Akhter, W. J. Clegg, and A. F. Routh (2010), Evolution of mudcrack patterns during repeated drying cycles, *Soft Matter*, *6*, 3562–3567.
Goetz, L. K. (1980), Giant Desiccation Polygons in Wildhorse Flat, in *Fall Field Conference Guidebook 31, Trans Pecos Region*, edited by P. W. Dickerson, J. M. Hoffer, and J. F. Callender, pp. 285–287, New Mexico Geological Society (pp. 308).
Grauby, O., S. Petit, A. Decarreau, and A. Baronnet (1994), The nontronitesaponite series: An experimental approach, *Eur. J. Mineral.*, *6*, 99–112.
Grotzinger, J. P., et al. (2014), A habitable fluvio-lacustrine environment at Yellowknife Bay, Gale Crater, Mars, *Science*, *343*(6169), doi:10.1126/science.1242777.
Hardie, L. A. (1968), The origin of the recent non-marine evaporite deposit of Saline Valley, Inyo County, California, *Geochim. Cosmochim. Acta*, *32*, 1279–1301.
Hunt, G. R. (1977), Spectral signatures of particulate minerals in the visible and near infrared, *Geophysics*, *42*(3), 501–513, doi:10.1190/1.1440721.
Hunt, G. R., and J. W. Salisbury (1970), Visible and near infrared spectra of minerals and rocks, I, Silicate minerals, *Mod. Geol.*, *1*, 283–300.
Jachens, R. C., and V. E. Langenheim (2014), Gravity survey and interpretation of Fort Irwin and vicinity, Mojave Desert, California, chap. H of Buesch, D. C., ed., Geology and geophysics applied to groundwater hydrology at Fort Irwin, California, *U.S. Geol. Surv. Open File Rep., 2013–1024*, p.11, doi:10.3133/ofr20131024H.
Jayko, A. S. (2005), Late Quaternary denudation, Death and Panamint Valleys, eastern California, *Earth Sci. Rev.*, *73*, 271–289.
Jones, B. F. (1965), The hydrology and mineralogy of Deep Springs Lake Inyo County, California, *U.S. Geol. Surv. Prof. Pap., 502-A*.
Lorenz, R. D., and B. K. Jackson (2014), Declining rock movement at Racetrack Playa, Death Valley National Park: An indicator of climate change?, *Geomorphology*, *211*, 116–120.
Lorenz, R. D., B. Jackson, and A. Hayes (2010), Racetrack and Bonnie Claire: Southwestern US playa lakes as analogs for Ontario Lacus, Titan, *Planet. Space Sci.*, *58*, 724–731.
Lorenz, R. D., B. K. Jackson, J. B. Barnes, J. N. Spitale, J. Radebaugh, and K. H. Baines (2011), Meteorological conditions at Racetrack Playa, Death Valley National Park: Implications for rock production and transport, *J. Appl. Meteorol. Climatol.*, *50*, 2361–2375.
Lynch, K. L., B. H. Horgan, J. Munakata-Marr, J. Hanley, R. J. Schneider, K. A. Rey, J. R. Spear, W. A. Jackson, and S. M. Ritter (2015), Near-infrared spectroscopy of lacustrine sediments in the Great Salt Lake Desert: An analog study for Martian paleolake basins, *J. Geophys. Res. Planets*, *120*, 599–623, doi:10.1002/2014JE004707.
McCave, I. N., and J. P. M. Syvitski (Eds.) (1991), *Principles, Methods and Application of Particle Size Analysis*, 388 pp., Cambridge Univ. Press, New York.
McEwen, A. S., et al. (2007), Mars Reconnaissance Orbiter's High Resolution Imaging Science Experiment (HiRISE), *J. Geophys. Res.*, *112*, E05S02, doi:10.1029/2005JE002605.
McKeown, N. K., J. L. Bishop, and E. A. Silver (2013), Variability of rock texture and morphology correlated with the clay-bearing units at Mawrth Vallis, Mars, *J. Geophys. Res. Planets*, *118*, 1245–1256, doi:10.1002/jgre.20096.
McLennan, S. M., et al. (2005), Provenance and diagenesis of the evaporite-bearing Burns formation, Meridiani Planum, Mars, *Earth Planet. Sci. Lett.*, *240*, 95–121, doi:10.1016/j.epsl.2005.09.041.
Messina, P., and P. Stoffer (2000), Terrain analysis of the Racetrack basin and the sliding rocks of Death Valley, *Geomorphology*, *35*, 253–265.
Messina, P., P. Stoffer, and W. C. Smith (2005), Macropolygon morphology, development, and classification on North Panamint and Eureka playas, Death Valley National Park CA, *Earth Sci. Rev.*, *73*, 309–322.
Miller, G. A. (1977), Appraisal of the water resources of Death Valley, California-Nevada, *U.S. Geol. Surv. Open File Rep., 77–728*.
Motts, W. S., and D. Carpenter (1968), Report of test drilling on Rogers, Coyote, Rosamond, and Panamint Playas in 1966, in *Playa Surface Morphology: Miscellaneous Investigations, Office of Aerospace Research*, edited by J. T. Neal, pp. 31–57, Air Force Cambridge Research Laboratories, U.S. Air Force, Bedford, Mass.
Murchie, S., et al. (2007), Compact Reconnaissance Imaging Spectrometer for Mars (CRISM) on Mars Reconnaissance Orbiter (MRO), *J. Geophys. Res.*, *112*, E05S03, doi:10.1029/2006JE002682.
Neal, J. T., and W. S. Motts (1967), Recent geomorphic changes in playas of western United States, *J. Geol.*, *75*(5), 511–525.
Neal, J. T., A. M. Langer, and P. F. Kerr (1968), Giant desiccation polygons of Great Basin Playas, *Geol. Soc. Am. Bull.*, *79*, 69–90.

Norris, R., J. Norris, R. Lorenz, J. Ray and B. Jackson, (2014), Sliding rocks on Racetrack Playa, Death Valley National Park: First observation of rocks in motion, *PLoS One*, *9*(8), e105948, doi:10.1371/journal.pone.0105948.

Osterloo, M. M., et al. (2008), Chloride-bearing materials in the Southern Highlands of Mars, *Science*, *319*, 1651–1654, doi:10.1126/science.1150690.

Osterloo, M. M., F. S. Anderson, V. E. Hamilton, and B. M. Hynek (2010), Geologic context of proposed chloride-bearing materials on Mars, *J. Geophys. Res.*, *115*, E10012, doi:10.1029/2010JE003613.

Petit, S. J., A. Decarreau, and F. Martin (1999), Characterization of octahedral substitutions in kaolinites using near infrared spectroscopy, *Clays Clay Miner.*, *47*, 103–108, doi:10.1346/CCMN.1999.0470111.

Pommerol, A., B. Jost, O. Poch, M. R. El-Maarry, B. Vuitel, and N. Thomas (2015), Laboratory characterization of the sublimation of icy planetary analogues: First results of the SCITEAS experiment, *Planet. Space Sci.*, *109–110*, 106–122.

Reid, J. B., E. P. Bucklin, L. Copenagle, J. Kidder, S. M. Pack, P. J. Polissar, and M. J. Williams (1995), Sliding rocks at the Racetrack, Death Valley: What makes them move?, *Geology*, *23*, 819–822.

Rubin, A. E., R. S. Verish, C. B. Moore, and R. A. Oriti (2000), Numerous unpaired meteorites exposed on a deflating playa lake at Lucerne Valley, California, *Meteorit. Planet. Sci.*, *35*, A181–A183.

Ruesch, O., F. Poulet, M. Vincendon, J.-P. Bibring, J. Carter, G. Erkeling, B. Gondet, H. Hiesinger, A. Ody, and D. Reiss (2012), Compositional investigation of the proposed chloride-bearing materials on Mars using near-infrared orbital data from OMEGA/MEx, *J. Geophys. Res.*, *117*, E00J13, doi:10.1029/2012JE004108.

Ryzak, M., and A. Bieganoski (2011), Methodological aspects of determining soil particle-size distribution using the laser diffraction method, *J. Plant Nutr. Soil Sci.*, *174*, 624–633.

Sharp, R. P., and D. L. Carey (1976), Sliding stones, Racetrack Playa, California, *Geol. Soc. Am. Bull.*, *87*, 1704–1717.

Tang, C. S., B. Shi, C. Liu, L. Zhao, and B. Wang (2008), Influencing factors of geometrical structure of surface shrinkage cracks in clayey soils, *Eng.Geol.*, *101*, 204–217.

Tang, C. S., Y. Y. Cui, B. Shi, A. M. Tang, and C. Liu (2011), Desiccation and cracking behavior of clay layer from slurry state under wetting-drying cycles, *Geoderma*, *166*, 111–118.

Teague, N. F., C. L. Stamos, S. F. House, and D. A. Clark (2014), Regional water table (2012) in the Mojave River and Morongo groundwater basins, southwestern Mojave Desert, California, USGS Data Release, doi:10.5066/F7CJ8BHF.

Watters, W. A., et al. (2011), Origin of the structure and planform of small impact craters in fractured targets: Endurance crater at Meridiani Planum, Mars, *Icarus*, *211*, 472–497, doi:10.1016/j.icarus.2010.08.030.

Wray, J. J., S. W. Squyres, L. H. Roach, J. L. Bishop, J. F. Mustard, and E. Z. Noe Dobrea (2010), Identification of the Ca-sulfate bassanite in Mawrth Vallis, Mars, *Icarus*, *209*, 406–421.

Wray, J. J., et al. (2011), Columbus crater and other possible groundwater-fed paleolakes of Terra Sirenum, Mars, *J. Geophys. Res.*, *116*, E01001, doi:10.1029/2010JE003694.